A direct approach for three-dimensional elasto-static and elasto-dynamic solutions in curvilinear cylindrical coordinates with application to classical

European Journal of Mechanics / A Solids 95 (2022) 104646

Contents lists available at ScienceDirect

European Journal of Mechanics / A Solids

journal homepage: www.elsevier.com/locate/ejmsol

A direct approach for three-dimensional elasto-static and elasto-dynamic solutions in curvilinear cylindrical coordinates with application to classical cylinder problems

Seyed Rasoul Atashipour [a,b,*], Zahra Mohammadi [c], Peter D. Folkow [a]

[a] Division of Dynamics, Department of Mechanics and Maritime Sciences (M2), Chalmers University of Technology, SE-412 96, Gothenburg, Sweden
[b] NVH and Experimental Mechanics Laboratory, Department of Mechanical Engineering, Kettering University, 1700 University Ave, Flint, MI, 48504, USA
[c] Babol Noshirvani University of Technology, Civil Engineering Department, Babol, Mazandaran, 47148-71167, Iran

ARTICLE INFO

Keywords:
Three-dimensional elasticity representation
New solution approach
Curvilinear cylindrical coordinates
Exact solution
Solid and thick-walled finite cylinders

ABSTRACT

This paper deals with introducing a unique representation of the three-dimensional Navier's equations of motion in cylindrical coordinate system in an exact simplified form without any approximation, aiming at facilitating solution procedure for different 3-D elasto-static and elasto-dynamic problems in the future. A novel form of the 3-D elasticity equations of motion including the body forces in cylindrical coordinate system is derived in an uncoupled form in terms of the longitudinal (axial) displacement component and the 'r-θ' in-plane anti-symmetric rotation function instead of introducing any additional auxiliary unknown potential function. The other displacement components (i.e., circumferential and radial displacement components) are shown to be obtained from two independent equations in terms of the determined axial displacement and the aforementioned rotation component. The correctness, validity and easy implementation of the introduced elasticity approach for obtaining exact elasticity solutions for various 3-D elasto-static and elasto-dynamic problems are demonstrated through solving a number of known elasticity problems. Three-dimensional static and free vibrations of finite-length solid cylinders as well as thick-walled hollow cylindrical shells are analytically solved. Numerical comparative results and discussion are conducted. Excellent agreement between the obtained results and those reported in the literature is observed in all cases, confirming the validity of the proposed new approach.

1. Introduction

Due to the complexity and highly-coupled nature of the three-dimensional elasticity field equations, it is not easy and straightforward to implement solutions for different problems within the area of elastic solid and structural mechanics. Thus, most solution strategies have been developed for reduced problems that typically include axisymmetry assumption or two-dimensionality to simplify particular aspects of the formulation and corresponding solution scheme.

When dealing with the reduced 2-D plane-stress/strain problems or treating thin-walled elastic structures, there have been introduced various efficient solution approaches based on an uncoupled representation of the governing equations in literature. For the sake of 2-D symmetric/plane-stress/strain elasticity, the well-known uncoupling stress-based formulation and solution scheme of the Airy stress function in conjunction with the 2-D Beltrami-Michell and their completeness (Chou and Pagano, 2013; Kaljevic et al., 1994) are commonly referred. Another well-known stress-based potential function approach is that of Prandtl's (Prandtl, 1903), specifically used for torsion problems and the Saint-Venant effects; see e.g. Ecsedi and Baksa (2010). For the 2-D displacement-based elasticity, the known Kolosov-Muskhelishvili potentials and complex variable solutions (Muskhelishvili, 1963) may be referred. A detailed review and complete picture of the history and development of 2-D plane elasticity theory is presented by Teodorescu (1964).

Treating thin-walled elastic structures, also several uncoupling potential function based 2-D solution approaches have been developed in the past decades for different thin to moderately-thick plate and shell theories; e.g., see the work of Nosier and his co-workers (Nosier et al., 2001a, 2001b) for the static equations of the first-order shear

* Corresponding author. NVH and Experimental Mechanics Laboratory, Department of Mechanical Engineering, Kettering University, 1700 University Ave, Flint, MI, 48504, USA.
E-mail addresses: rasoul.atashipour@chalmers.se, ratashipour@kettering.edu (S.R. Atashipour).

https://doi.org/10.1016/j.euromechsol.2022.104646
Received 21 February 2022; Received in revised form 13 April 2022; Accepted 4 May 2022
Available online 11 May 2022

deformation theory (FSDT), the so-called Mindlin-Reissner theory, in Cartesian and polar coordinates. For the dynamic equations and vibration solutions of elastic plates and shells see Hosseini-Hashemi and Arsanjani, 2005; Jomehzadeh and Saidi, 2009; Hosseini-Hashemi et al., 2012; and for the static and dynamic problems of elastic plates and shells based on the higher-order shear deformation theory (HSDT) (also known as Reddy's theory) see Atashipour et al., 2010; Hosseini Hashemi et al., 2012; Hosseini-Hashemi et al., 2012. With regard to accurate analysis of thick plates, a proprietary thick plate hypothesis, based on introducing a complex higher-order displacement field, was developed by Kaprielian, Rogers and Spencer (Kaprielian et al., 1988). The origins of the method can be found in the classical solutions by Michell (1899) for stresses in moderately thick elastic plates, and a reformulation of 3-D Michell's equations. Several thick plate problems have recently been analyzed based on the mentioned approach (England, 2006; Yang et al., 2012; Shen et al., 2022).

A series of extensions of the 2-D elasticity groundwork has recently been carried out with regard to non-homogeneity and functionally grading (FG) material effects, non-isotropic/composite directional material property effects of constituents, and/or micro-/nano-scale medium effects (see e.g., Lazar and Maugin, 2005; Lazar et al., 2006; Ecsedi, 2009; Ecsedi and Baksa, 2010; Ecsedi, 2013; Chu et al., 2015).

Whilst the vast majority of the 2-D elastic hypotheses are incapable of capturing structural behavior of solid and thick-walled members, the more complex 3-D elasticity theory need to be employed for the analysis of different elasto-static and elasto-dynamic problems. Considering the difficulty associated with obtaining solutions based on the 3-D elasticity, much effort has been devoted by researchers in the field in the past decades to establish new formulation and solution schemes for the original Navier's governing equations in a simpler displacement-based or stress-based format. Evidently, almost all the existing approaches are on the basis of introducing some physically-meaningless auxiliary potential functions (known as methods of potentials). One of the most important displacement-based 3-D elasticity solution approaches is the well-known Helmholtz vector representation (the so-called Helmholtz decomposition) in which the displacement vector is represented as the sum of the gradient of a scalar potential plus the curl of a vector potential (Peckhold, 1971). Apparently, as a special case of the Helmholtz decomposition approach, in absence of body forces and limiting the solution scheme to be only based on scalar potential, the known Lamé's strain potential approach is deduced. Galerkin (1930) established a 3-D vector potential representation, describing the displacement components in terms of the second derivatives of a vector potential function, only. The 3-D Love's strain potential approach (Love, 1927) can also be derived as a special case of the Galerkin potential method, assuming zero body forces and eliminating the two planar components of the potential vector. A powerful general displacement-based solution approach to the 3-D Navier's elasticity equations was developed by Papkovich (1932) and Neuber (1934), commonly referred to as Papkovich-Neuber representation. From the ground well-known 3-D stress-based solution approaches, the potential methods of Beltrami, Maxwell and Morera representations can be pointed out; see Chou and Pagano (2013) for details. Apparently, all the mentioned 3-D approaches are limited to the elasto-statics.

Several extended versions of the aforementioned ground 3-D elasticity approaches have been established taking into account the effect of non-homogeneity and non-isotropy of the elastic constituents; see e.g. Hu (1953), Nowacki (1954), Lekhnitskii and Lekhnitskii-Hu-Nowacki (Wang and Wang, 1995) for transversely isotropic material; and Plevako (1971) for inhomogeneous elastic media. Recently, an extension of the Lekhnitskii-Hu-Nowacki approach from the elastostatics to elasto-dynamics is performed by Eskandari-Ghadi (2005).

Apparently, the aim of all the above-mentioned potential decomposition approaches has been to avoid the difficulty in dealing with the original highly-coupled partial differential governing equations of the three-dimensional elasticity theory for solving different elasto-static and elasto-dynamic problems. However, decomposition representations are established at the expense of presenting the governing equations in terms of some new unknown potential functions, which may be difficult to initiate a solution based on a semi-inverse (see Sadd, 2009) methodology, as those potential functions are physically meaningless. Moreover, for all the 3-D displacement- or stress-based potential approaches, their solution schemes have always raised up the questions regarding the commonly-referred "completeness issue". Furthermore, several of them are lacking the ability of capturing the dynamic effects and the body forces. Atashipour and his colleagues (see Saidi et al., 2009) introduced a new reformulation of the original elasticity theory in an uncoupled form without introducing any auxiliary potential function in the Cartesian coordinate system, and based on that, exact closed-from solutions for bending and free vibration of thick rectangular plates are presented.

In this paper, an efficient solution approach is established for 3-D elasto-static and elasto-dynamic problems in the curvilinear cylindrical coordinate system based on decomposition of the 3-D elasticity equations of motion including the body forces without introducing any additional unknown potential function. The original governing equations of motion of the 3-D elasticity theory in cylindrical coordinates are recast into an uncoupled form in terms of a displacement and a rotation component without any approximation. To demonstrate validity and easiness of the presented approach for solving different elasto-static and elasto-dynamic problems, some classical problems in the cylindrical coordinate system are exactly solved, including the 3-D free vibration of both solid and thick-walled cylinders, as well as the 3-D static stresses in thick-walled cylindrical pressure vessels and the 3-D static analysis of stocky simply-supported beams with solid circular cross-section subjected to a distributed transverse load. The results are compared with those available in literature and corresponding 3-D finite element (FE) simulations.

2. Reformulation of the 3-D Navier equations of motion

2.1. Original form of the equations in cylindrical coordinate system

In general, the three-dimensional elasto-dynamic equations including the body forces are expressed as

$$\mu\nabla^2\vec{u}+(\lambda+\mu)\nabla(\nabla.\vec{u})+\vec{F}=\rho\ddot{\vec{u}} \tag{1}$$

in which $\vec{u}$ is the displacement vector and $\vec{F}$ is the vector of the body force (per unit volume); λ and μ are respectively the Lamé's coefficient and the shear modulus, and ρ is the mass density. They are expressed in terms of the modulus of elasticity, E, and the Poisson's ratio, ν as

$$\lambda=\frac{\nu E}{(1+\nu)(1-2\nu)}$$
$$\mu=\frac{E}{2(1+\nu)} \tag{2}$$

Also, ∇^2 and ∇ are the Laplace operator and the gradient, respectively, and are represented in the cylindrical coordinate system as

$$\nabla^2=\frac{1}{r}\frac{\partial}{\partial r}\left(r\frac{\partial}{\partial r}\right)+\frac{1}{r^2}\frac{\partial^2}{\partial\theta^2}+\frac{\partial^2}{\partial z^2}$$
$$\nabla=\frac{\partial}{\partial r}\hat{\mathbf{r}}+\frac{1}{r}\frac{\partial}{\partial\theta}\hat{\boldsymbol{\theta}}+\frac{\partial}{\partial z}\hat{\mathbf{z}} \tag{3}$$

Expanding Eq. (1) in the cylindrical coordinate system, the set of three-dimensional elasticity equations for a linear elastic isotropic material is written in the form

$$
\begin{aligned}
&(\lambda+2\mu)\left(u_{r,rr}+\frac{1}{r}u_{r,r}-\frac{1}{r^2}u_r\right)+\mu\frac{1}{r^2}u_{r,\theta\theta}+\mu u_{r,zz}+(\lambda+\mu)\left(\frac{1}{r}u_{\theta,r\theta}+\frac{1}{r^2}u_{\theta,\theta}\right)-2(\lambda+2\mu)\frac{1}{r^2}u_{\theta,\theta}+(\lambda+\mu)u_{z,rz}+F_r=\rho\ddot{u}_r\\
&\mu\left(u_{\theta,rr}+\frac{1}{r}u_{\theta,r}-\frac{1}{r^2}u_\theta\right)+(\lambda+2\mu)\frac{1}{r^2}u_{\theta,\theta\theta}+\mu u_{\theta,zz}+(\lambda+\mu)\left(\frac{1}{r}u_{r,r\theta}-\frac{1}{r^2}u_{r,\theta}\right)+2(\lambda+2\mu)\frac{1}{r^2}u_{r,\theta}+(\lambda+\mu)\frac{1}{r}u_{z,\theta z}+F_\theta=\rho\ddot{u}_\theta\\
&\mu\left(u_{z,rr}+\frac{1}{r}u_{z,r}+\frac{1}{r^2}u_{z,\theta\theta}\right)+(\lambda+2\mu)u_{z,zz}+(\lambda+\mu)\left(u_{r,rz}+\frac{1}{r}u_{r,z}\right)+(\lambda+\mu)\frac{1}{r}u_{\theta,\theta z}+F_z=\rho\ddot{u}_z
\end{aligned}
\tag{4}
$$

in which the comma in the subscript indicates the derivative with respect to the variables following it. Obviously, due to the highly-coupled nature of the above equations, gaining exact solutions for different static and dynamic problems within the area of solid mechanics is mathematically difficult. Therefore, it is reasonable to recast them in an uncoupled simpler form in terms of the known physical functions.

2.2. Recasting the original equations into an uncoupled form

The original set of three-dimensional Navier equations of motion (4), after some mathematical manipulation, can be rewritten as

$$
\begin{aligned}
&\eta\left(u_{r,rr}+\frac{1}{r}u_{r,r}-\frac{1}{r^2}u_r\right)+\mu\frac{1}{r^2}u_{r,\theta\theta}+(\eta-\mu)\frac{1}{r}u_{\theta,r\theta}-(\eta+\mu)\frac{1}{r^2}u_{\theta,\theta}+(\eta-\mu)u_{z,rz}\\
&\qquad+\mu u_{r,zz}+F_r=\rho\ddot{u}_r
\end{aligned}
\tag{5a}
$$

$$
\begin{aligned}
&\mu\left(u_{\theta,rr}+\frac{1}{r}u_{\theta,r}-\frac{1}{r^2}u_\theta\right)+\eta\frac{1}{r^2}u_{\theta,\theta\theta}+(\eta-\mu)\frac{1}{r}u_{r,r\theta}+(\eta+\mu)\frac{1}{r^2}u_{r,\theta}+(\eta-\mu)\frac{1}{r}u_{z,\theta z}\\
&\qquad+\mu u_{\theta,zz}+F_\theta=\rho\ddot{u}_\theta
\end{aligned}
\tag{5b}
$$

$$
\mu\nabla^2_{r\theta}u_z+(\eta-\mu)\left(u_{r,rz}+\frac{1}{r}u_{r,z}\right)+(\eta-\mu)\frac{1}{r}u_{\theta,\theta z}+\eta u_{z,zz}+F_z=\rho\ddot{u}_z \tag{5c}
$$

where $\nabla^2_{r\theta}$ is the two-dimensional Laplace operator in $r-\theta$ polar plane; i.e.,

$$
\nabla^2_{r\theta}=\frac{\partial^2}{\partial r^2}+\frac{1}{r}\frac{\partial}{\partial r}+\frac{1}{r^2}\frac{\partial^2}{\partial\theta^2} \tag{6}
$$

and η is a material constant, defined as

$$
\eta=\frac{(1-\nu)E}{(1+\nu)(1-2\nu)} \tag{7}
$$

Now, we define two differential operators as follows:

$$
\begin{aligned}
&\hat{d}_1=\partial/\partial r+1/r\\
&\hat{d}_2=(1/r)(\partial/\partial\theta)
\end{aligned}
\tag{8}
$$

Adding the two Eqs. (5a) and (5b) together after using the operations $\hat{d}_1$ and $\hat{d}_2$, respectively, and then rewriting Eq. (5c) in terms of $(\hat{d}_1u_r+\hat{d}_2u_\theta)$ yield

$$
\eta\nabla^2_{r\theta}V^s_{2D}+\mu V^s_{2D,zz}+(\eta-\mu)\nabla^2_{r\theta}u_{z,z}+\left(F_{r,r}+\frac{1}{r}F_r+\frac{1}{r}F_{\theta,\theta}\right)=\rho\ddot{V}^s_{2D} \tag{9a}
$$

$$
\mu\nabla^2_{r\theta}u_z+\eta u_{z,zz}+(\eta-\mu)V^s_{2D,z}+F_z=\rho\ddot{u}_z \tag{9b}
$$

where V^s_{2D} is the two-dimensional volumetric strain in the radial-circumferential plane, i.e.,

$$
V^s_{2D}=\nabla_{r\theta}.\mathbf{u}=\varepsilon_{rr}+\varepsilon_{\theta\theta}=\hat{d}_1u_r+\hat{d}_2u_\theta=u_{r,r}+\frac{1}{r}u_{\theta,\theta}+\frac{1}{r}u_r \tag{10}
$$

Eliminating V^s_{2D} from Eq. (9a,b) results in an independent fourth-order equation in term of the longitudinal displacement component, u_z as

$$
\begin{aligned}
&\nabla^4u_z-\rho\left(\frac{1}{\mu}+\frac{1}{\eta}\right)\nabla^2\ddot{u}_z+\frac{\rho^2}{\mu\eta}\ddot{\ddot{u}}_z=-\frac{1}{\mu}\nabla^2F_z+\left(\frac{1}{\mu}-\frac{1}{\eta}\right)\left(F_{r,r}+\frac{1}{r}F_r+\frac{1}{r}F_{\theta,\theta}+F_{z,z}\right)_{,z}\\
&\qquad+\frac{\rho}{\mu\eta}\ddot{F}_z
\end{aligned}
\tag{11}
$$

Now, we apply $\hat{d}_2$ and $\hat{d}_1$ to Eqs. (5a) and (5b), respectively, and subtract the results and obtain:

$$
\nabla^2\omega_{r\theta}-\frac{\rho}{\mu}\ddot{\omega}_{r\theta}=\frac{1}{\mu}\left(F_{\theta,r}-\frac{1}{r}F_{r,\theta}+\frac{1}{r}F_\theta\right) \tag{12}
$$

where $\omega_{r\theta}$ is the anti-symmetric component of rotation tensor in $r-\theta$ plane; i.e.,

$$
\omega_{r\theta}=\frac{1}{2}\left(\frac{1}{r}u_{r,\theta}-u_{\theta,r}-\frac{1}{r}u_\theta\right) \tag{13}
$$

It can be clearly seen from Eqs. (11) and (12) that the total degree/order of the mentioned equations is identical to that of the original Navier equations of motion. Apparently, the two mentioned uncoupled equations presented by Eqs. (11) and (12) in terms of the longitudinal displacement component, u_z, and the anti-symmetric rotation component, $\omega_{r\theta}$, respectively, can be used as a replacement of the original Navier equations of motion in cylindrical coordinate system, without any approximation, for solving different dynamic problems within the frame of the linear elasticity for isotropic materials. In case of static problems, the aforementioned two equations in absence of the body forces are simplified in the form:

$$
\nabla^4u_z=0 \tag{14a}
$$

$$
\nabla^2\omega_{r\theta}=0 \tag{14b}
$$

To be able to solve an elasto-static or elasto-dynamic problem based on the new approach, other components of the displacement vector (i.e., u_r and u_θ) should also be determined. To this end, some additional equations are introduced in the following to express them in terms of the two parameters u_z and $\omega_{r\theta}$.

2.3. Specification of the displacement components

As mentioned earlier, the longitudinal displacement and the anti-symmetric rotation components can be obtained independently by solving the uncoupled equations (11) and (12), respectively. To achieve a complete solution for any elasticity problem using the new approach, other components of the displacement vector, i.e., the radial and circumferential displacements, should also be determined. In the following, some equations, describing the mentioned displacement components in terms of u_z and $\omega_{r\theta}$, are introduced.

To start, we differentiate Eq. (13) once with respect to θ and next with respect to r, and rewrite them for the terms $u_{\theta,r\theta}$ and $u_{r,r\theta}$ as

$$u_{\theta,r\theta} = -2\omega_{r\theta,\theta} + \frac{1}{r}u_{r,\theta\theta} - \frac{1}{r}u_{\theta,\theta} \tag{15a}$$

$$u_{r,r\theta} = 2r\omega_{r\theta,r} + ru_{\theta,rr} + u_{\theta,r} - \frac{1}{r}u_{\theta} + \frac{1}{r}u_{r,\theta} \tag{15b}$$

Substituting Eqs. (15a) and (15b) into Eqs. (5a) and (5b), respectively, and simplifying the results yield:

$$\eta\left(\nabla^2_{r\theta}u_r - \frac{1}{r^2}u_r - \frac{2}{r^2}u_{\theta,\theta}\right) - 2(\eta-\mu)\frac{1}{r}\omega_{r\theta,\theta} + (\eta-\mu)u_{z,rz} + \mu u_{r,zz} + F_r = \rho\ddot{u}_r \tag{16a}$$

$$\eta\left(\nabla^2_{r\theta}u_\theta - \frac{1}{r^2}u_\theta + \frac{2}{r^2}u_{r,\theta}\right) + 2(\eta-\mu)\omega_{r\theta,r} + (\eta-\mu)\frac{1}{r}u_{z,\theta z} + \mu u_{\theta,zz} + F_\theta = \rho\ddot{u}_\theta \tag{16b}$$

Also, differentiating Eq. (5c) once with respect to r and next with respect to θ, and eliminating the terms $u_{\theta,r\theta z}$ and $u_{r,r\theta z}$ from the resulted equations, respectively, using Eqs. (15a) and (15b), will result in the following equations:

$$(\eta-\mu)\left(\nabla^2_{r\theta}u_r - \frac{1}{r^2}u_r - \frac{2}{r^2}u_{\theta,\theta}\right)_{,z} - 2(\eta-\mu)\frac{1}{r}\omega_{r\theta,\theta z} + (\eta-\mu)u_{z,rzz} + \mu\left(\nabla^2 u_z\right)_{,r} + F_{z,r} = \rho\ddot{u}_{z,r} \tag{17a}$$

$$(\eta-\mu)r\left(\nabla^2_{r\theta}u_\theta - \frac{1}{r^2}u_\theta + \frac{2}{r^2}u_{r,\theta}\right)_{,z} + 2(\eta-\mu)r\omega_{r\theta,rz} + (\eta-\mu)u_{z,\theta zz} + \mu\left(\nabla^2 u_z\right)_{,\theta} + F_{z,\theta} = \rho\ddot{u}_{z,\theta} \tag{17b}$$

where ∇^2 is the 3-D Laplace operator and is given by Eq. (3). Now, we eliminate the differential term $(\nabla^2_{r\theta}u_r - u_r/r^2 - 2u_{\theta,\theta}/r^2)$ from Eqs. (16a) and (17a), and then eliminate the differential term $(\nabla^2_{r\theta}u_\theta - u_\theta/r^2 + 2u_{r,\theta}/r^2)$ from Eqs. (16b) and (17b), and obtain two independent differential equations for the undetermined displacement functions u_r and u_θ as follows:

$$u_{r,zzz} - \frac{\rho}{\mu}\ddot{u}_{r,z} = \frac{\eta}{\mu(\eta-\mu)}\left(\mu\nabla^2 u_z + \frac{\mu}{\eta}(\eta-\mu)u_{z,zz} - \rho\ddot{u}_z + F_z\right)_{,r} - \left(\frac{2}{r}\omega_{r\theta,\theta} + \frac{1}{\mu}F_r\right)_{,z} \tag{18a}$$

$$u_{\theta,zzz} - \frac{\rho}{\mu}\ddot{u}_{\theta,z} = \frac{\eta}{\mu(\eta-\mu)}\frac{1}{r}\left(\mu\nabla^2 u_z + \frac{\mu}{\eta}(\eta-\mu)u_{z,zz} - \rho\ddot{u}_z + F_z\right)_{,\theta} + \left(2\omega_{r\theta,r} - \frac{1}{\mu}F_\theta\right)_{,z} \tag{18b}$$

Eqs. (18a) and (18b) express the displacement component u_r and u_θ in terms of u_z and $\omega_{r\theta}$; which are simplified for elasto-statics problems in absence of the body forces as

$$u_{r,zzz} = \left(\frac{\eta}{\eta-\mu}\nabla^2 u_z + u_{z,zz}\right)_{,r} - \frac{2}{r}\omega_{r\theta,\theta z} \tag{19a}$$

$$u_{\theta,zzz} = \frac{1}{r}\left(\frac{\eta}{\eta-\mu}\nabla^2 u_z + u_{z,zz}\right)_{,\theta} + 2\omega_{r\theta,rz} \tag{19b}$$

To show validity and efficiency of the proposed new approach, especially in gaining analytical solutions, some known three-dimensional static and free vibration problems of solid and hollow thick-walled cylinders are analytically solved in the next section.

3. Application to exact analytical solutions for classical cylinder problems

The three-dimensional analysis of solid cylinders and thick-walled hollow cylinders/cylindrical shells has been the subject of research for several decades. In many studies, the three-dimensional elasticity has been adopted in conjunction with various levels of approximations when studying solid cylinder problems with various different end boundary conditions. There exist on the one hand analytical solutions based on expansion in terms of Bessel functions (Hutchinson, 1980; Kari, 2002), and on the other hand numerical solutions such as e.g., Ritz method (Liew and Hung, 1995; Leissa and So, 1995). These works using approximate approaches concentrate mainly on eigen-natural frequency analyses. The three-dimensional free vibration of thick-walled cylindrical shells have been studied by several researchers (Gazis, 1958; Armenakas et al., 1969), but the bulk of analyses has been on various approximate models or have been conducted for simplified symmetric/plane-strain conditions due to the complexity of the exact solutions.

In the following, exact analytical easlto-static and elasto-dynamic solutions are conducted for some static and vibration problems of both finite-length solid cylinders and thick-walled cylindrical shells on the basis of the introduced 3-D representation.

3.1. Exact elasto-static solutions

Consider a thick-walled hollow circular cylinder of inner and outer radii a and b, respectively, and length L. The thick-walled cylinder is assumed to be simply-supported at both ends (i.e., at $z = 0, L$) and is in a general state subjected to an arbitrarily distributed internal load of intensity $p_i(\theta, z)$, and externally is under an arbitrary load of intensity $p_o(\theta, z)$ as shown in Fig. 1.

Based on the separation of variables method, the solution for the displacement component along the z direction as well as the antisymmetric rotation component $\omega_{r\theta}$, using the double Fourier series, are represented as

$$u_z = \sum_{m=0}^{\infty}\sum_{n=0}^{\infty} U_{z\,mn}(r)\cos n\theta \cos\alpha_m z \tag{20a}$$

$$\omega_{r\theta} = \sum_{m=1}^{\infty}\sum_{n=1}^{\infty} \Omega_{r\theta\,mn}(r)\sin n\theta \sin\alpha_m z \tag{20b}$$

where $U_{z\,mn}(r)$ and $\Omega_{r\theta\,mn}(r)$ are two unknown functions of the radial variable, r, only; n is the number of half-waves superimposed to describe the deformed shape in the circumferential direction, and $\alpha_m = m\pi/L$ indicates the deformed shape of the cylinder along the longitudinal direction. It should be pointed out that the trigonometric functions of θ and z in Eq. (20a,b) satisfy the continuity of a closed cylinder in the hoop direction, as well as the simply-supported end boundary conditions (see also the resultant displacements u_r and u_θ, and the stress components in the following) which are expressed as:

$$\sigma_{zz}|_{z=0,L} = u_r|_{z=0,L} = u_\theta|_{z=0,L} = 0 \tag{21}$$

Substituting Eqs. (20a) and (20b) into Eqs. (14a) and (14b),

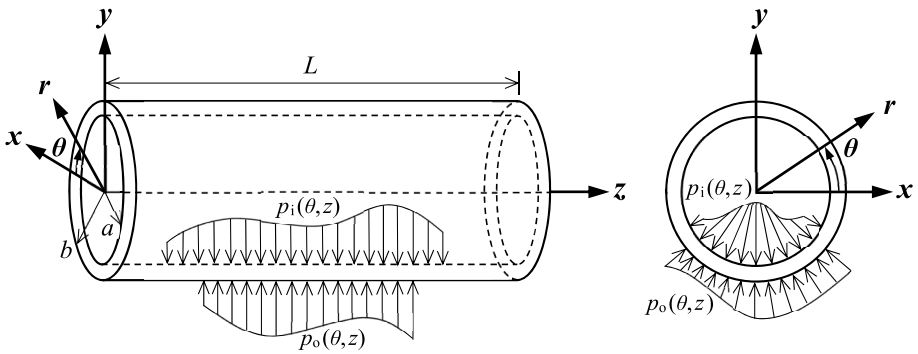

Fig. 1. Thick-walled closed cylinders subjected to arbitrary distributed internal and external loading.

respectively, will result in the following two independent ordinary differential equations:

$$U^{(4)}_{z\,mn}(r)+\frac{2}{r}U'''_{z\,mn}(r)-\frac{1}{r^2}\left(1+2n^2+2\alpha_m^2r^2\right)U''_{z\,mn}(r)+\frac{1}{r^3}\left(1+2n^2-2\alpha_m^2r^2\right)U'_{z\,mn}(r)+\frac{1}{r^4}\left(n^4-4n^2+2n^2\alpha_m^2r^2+\alpha_m^4r^4\right)U_{z\,mn}(r)=0 \tag{22a}$$

$$\Omega''_{r\theta\,mn}+\frac{1}{r}\Omega'_{r\theta\,mn}-\frac{1}{r^2}\left(n^2+\alpha_m^2r^2\right)\Omega_{r\theta\,mn}=0 \tag{22b}$$

The exact solutions of the ordinary differential Eq. (22a,b) can be expressed in terms of the modified Bessel functions of the first and second kind as

$$U_{z\,mn}(r)=[c_{1mn}I_n(\alpha_m r)+c_{2mn}K_n(\alpha_m r)]+r[c_{3mn}I_{n+1}(\alpha_m r)+c_{4mn}K_{n+1}(\alpha_m r)] \tag{23a}$$

$$\Omega_{r\theta\,mn}(r)=c_{5mn}I_n(\alpha_m r)+c_{6mn}K_n(\alpha_m r) \tag{23b}$$

where c_{1mn} through c_{6mn} are six coefficients to be determined from satisfaction of the boundary conditions at the internal and external surfaces of the thick-walled cylinder. Also, substituting Eqs. (20a) and (20b) into Eqs. (19a) and (19b) and integrating three times with respect to the variable z, other displacement components in the radial and circumferential directions are obtained as

$$u_r=\sum_{m=1}^{\infty}\sum_{n=0}^{\infty}U_{r\,mn}(r)\cos n\theta\,\sin\alpha_m z \tag{24a}$$

$$u_\theta=\sum_{m=1}^{\infty}\sum_{n=1}^{\infty}U_{\theta\,mn}(r)\sin n\theta\,\sin\alpha_m z \tag{24b}$$

in which

Next, all the strain and stress components can be determined by replacing the obtained exact closed-form equations for the displacement components into the linear strain-displacement relations in the cylindrical coordinate system as

$$\varepsilon_{rr}=u_{r,r},\quad \varepsilon_{\theta\theta}=\frac{1}{r}\left(u_r+u_{\theta,\theta}\right),\quad \varepsilon_{zz}=u_{z,z}$$
$$\varepsilon_{r\theta}=\frac{1}{2}\left(\frac{1}{r}u_{r,\theta}+u_{\theta,r}-\frac{1}{r}u_\theta\right),\quad \varepsilon_{\theta z}=\frac{1}{2}\left(u_{\theta,z}+\frac{1}{r}u_{z,\theta}\right),\quad \varepsilon_{rz}=\frac{1}{2}\left(u_{r,z}+u_{z,r}\right) \tag{26}$$

and afterwards replacing the results into the constitutive Hooke's law for the linear elastic isotropic material as follows

$$\sigma_{ij}=\lambda\varepsilon_{kk}\delta_{ij}+2\mu\varepsilon_{ij},\quad i,j\in\{r,\theta,z\} \tag{27}$$

where δ_{ij} is the Kronecker delta, and the Lamé's coefficients λ and μ are given by Eq. (2).

As mentioned earlier, the displacement field of Eq. (20a,b) satisfies the simply supported boundary conditions as well as the continuity of a hollow circular cylinder, and the remaining boundary conditions related to the internal and external surfaces need to be satisfied. In case that the cylinder is subjected to arbitrarily distributed internal and external load of intensity $p_i(\theta,z)$ and $p_o(\theta,z)$, respectively, the following boundary conditions need to be satisfied

$$\begin{aligned}&\sigma_{r\theta}|_{r=a}=\sigma_{r\theta}|_{r=b}=0\\&\sigma_{rz}|_{r=a}=\sigma_{rz}|_{r=b}=0\\&\sigma_{rr}|_{r=a}=-p_i(\theta,z)\\&\sigma_{rr}|_{r=b}=-p_o(\theta,z)\end{aligned} \tag{28}$$

where an arbitrarily distributed load $p(\theta,z)$ can be described using the double Fourier series in the form:

$$U_{r\,mn}=\frac{1}{\alpha_m}\Bigg\{\left[c_{1mn}I'_n(\alpha_m r)+c_{2mn}K'_n(\alpha_m r)\right]+\frac{2n}{\alpha_m r}\left[c_{5mn}I_n(\alpha_m r)+c_{6mn}K_n(\alpha_m r)\right]-\left(\frac{\eta}{\eta-\mu}\frac{2n}{\alpha_m^2r^2}-1\right)r\left[c_{3mn}I'_{n+1}(\alpha_m r)+c_{4mn}K'_{n+1}(\alpha_m r)\right]-\left[\frac{2\eta}{\eta-\mu}\left(1+\frac{n(n+1)}{\alpha_m^2r^2}\right)-1\right]\left[c_{3mn}I_{n+1}(\alpha_m r)+c_{4mn}K_{n+1}(\alpha_m r)\right]\Bigg\} \tag{25a}$$

$$U_{\theta\,mn}=-\frac{1}{\alpha_m}\Bigg\{\frac{n}{r}\left[c_{1mn}I_n(\alpha_m r)+c_{2mn}K_n(\alpha_m r)\right]+\frac{2}{\alpha_m}\left[c_{5mn}I'_n(\alpha_m r)+c_{6mn}K'_n(\alpha_m r)\right]-\frac{\eta}{\eta-\mu}\frac{2n}{\alpha_m r}\left[c_{3mn}I_n(\alpha_m r)-c_{4mn}K_n(\alpha_m r)\right]+n\left[c_{3mn}I_{n+1}(\alpha_m r)+c_{4mn}K_{n+1}(\alpha_m r)\right]\Bigg\} \tag{25b}$$

$$p(\theta,z)=\sum_{m=1}^{\infty}\sum_{n=0}^{\infty}P_{mn}\cos n\theta\sin\alpha_m z \tag{29}$$

in which

$$P_{m0}=\frac{2}{\pi L}\int_0^L\int_0^{\pi}p(\theta,z)\sin\alpha_m z\,\mathrm{d}\theta\,\mathrm{d}z,$$
$$P_{mn}=\frac{4}{\pi L}\int_0^L\int_0^{\pi}p(\theta,z)\cos n\theta\sin\alpha_m z\,\mathrm{d}\theta\,\mathrm{d}z,\quad (n\geq 1) \tag{30}$$

In the following, some practical examples are solved based on the presented analytical solutions.

$$u_z=\sum_{m=1,3,\ldots}^{\infty}\left[c_{1m}I_0(\alpha_m r)+c_{2m}K_0(\alpha_m r)\right]+r\left[c_{3m}I_1(\alpha_m r)+c_{4m}K_1(\alpha_m r)\right]\cos\alpha_m z \tag{33a}$$

$$\omega_{r\theta}=0 \tag{33b}$$

As a result, the other displacement components are given as

$$u_r=\sum_{m=1,3,\ldots}^{\infty}\left\{\frac{1}{\alpha_m}\left[c_{1m}I_0'(\alpha_m r)+c_{2m}K_0'(\alpha_m r)\right]-\frac{1}{\alpha_m}\left(\frac{2\eta}{\eta-\mu}-1\right)\left[c_{3m}I_1(\alpha_m r)+c_{4m}K_1(\alpha_m r)\right]+\frac{r}{\alpha_m}\left[c_{3m}I_1'(\alpha_m r)+c_{4m}K_1'(\alpha_m r)\right]\right\}\sin\alpha_m z \tag{34a}$$

$$u_\theta=0 \tag{34b}$$

Clearly, the shear stress components $\sigma_{r\theta}$ and $\sigma_{\theta z}$ become zero due to the axisymmetric condition and therefore the six boundary conditions by Eq. (28) are reduced to the following set of four algebraic equations:

3.1.1. Example 1 – thick-walled cylindrical vessel subjected to uniform internal pressure

Consider a thick-walled cylindrical vessel subjected to a uniformly distributed internal loading corresponding to a uniform pressure of intensity P_0. For this axisymmetric type of loading, the load coefficient by Eq. (30) is simplified as

$$P_{m0}=\frac{2P_0}{m\pi}[1-(-1)^m],\quad (n=0)$$
$$P_{mn}=0,\quad (n\geq 1) \tag{31}$$

and consequently, the distributed loading function by Eq. (29) is simplified in the form:

$$p_i(\theta,z)=\frac{4P_0}{\pi}\sum_{m=1,3,\ldots}^{\infty}\frac{1}{m}\sin\alpha_m z \tag{32}$$

Next, the displacement component u_z and the antisymmetric rotation component $\omega_{r\theta}$, from Eqs. (20) and (23) are expressed as

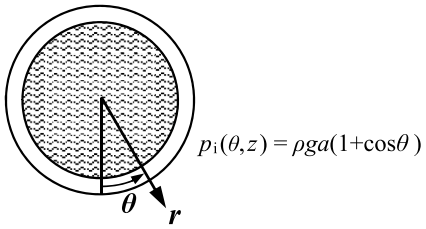

Fig. 2. Cross-section of a fully filled closed circular cylinder with inner and outer radii a and b, subjected to a non-uniform radial load from liquid pressure.

Table 1
Dimensionless displacements and stresses in thick-walled cylindrical vessels with various length- and thickness-to-average radius/diameter ratios, and comparison with the 2-D elasticity solution [The presented 3-D elasticity results are calculated based on 200 terms of the series to ensure the results' convergence].

h/R_0	Source	L/D_0	$z/L=0.5,\ r/a=1$			$z/L=0.5,\ r/a=1+h/a$		
			$Eu_r/(P_0h)$	σ_θ/P_0	σ_z/P_0	$Eu_r/(P_0h)$	σ_θ/P_0	σ_z/P_0
0.6	3-D Elasticity (Present)	1.0	2.572	1.660	−0.819	1.858	1.050	0.642
		1.2	2.681	1.840	−0.528	1.951	1.024	0.412
		1.5	2.683	1.933	−0.225	1.953	0.954	0.175
		2.0	2.575	1.908	−0.003	1.860	0.860	0.003
		5.0	2.469	1.818	0	1.769	0.817	0
		10.0	2.469	1.818	0	1.769	0.817	0
	2-D Elasticity[a] (Sadd, 2009)	–	2.469	1.817	0	1.769	0.817	0
0.8	3-D Elasticity (Present)	1.0	1.298	1.241	−0.638	0.774	0.583	0.468
		1.2	1.379	1.401	−0.461	0.843	0.583	0.337
		1.5	1.411	1.508	−0.249	0.871	0.552	0.181
		2.0	1.381	1.526	−0.055	0.845	0.495	0.040
		5.0	1.312	1.451	0	0.787	0.450	0
		10.0	1.312	1.451	0	0.788	0.450	0
	2-D Elasticity[a] (Sadd, 2009)	–	1.313	1.450	0	0.788	0.450	0
1.0	3-D Elasticity (Present)	1.0	0.745	1.055	−0.457	0.345	0.323	0.309
		1.2	0.792	1.181	−0.349	0.388	0.331	0.241
		1.5	0.818	1.274	−0.211	0.412	0.318	0.146
		2.0	0.813	1.305	−0.070	0.407	0.286	0.047
		5.0	0.775	1.251	0	0.375	0.250	0
		10.0	0.775	1.251	0	0.375	0.250	0
	2-D Elasticity[a] (Sadd, 2009)	–	0.775	1.250	0	0.375	0.250	0

[a] 2-D solution corresponding to end opened cylinder (i.e. plane stress solution).

$$\sigma_{rr}|_{r=a} = -\frac{4P_0}{\pi}\sum_{m=1,3,\ldots}^{\infty}\frac{1}{m}\sin\alpha_m z$$
$$\sigma_{rr}|_{r=b} = \sigma_{rz}|_{r=a} = \sigma_{rz}|_{r=b} = 0 \quad (35)$$

The coefficients c_{1m} through c_{4m} (in terms of m) are determined from the above-mentioned set of algebraic boundary equations.

Based on the presented solution, dimensionless numerical results are reported in Table 1 for the displacement and the stresses. It should be pointed out that $h = b - a$ is the thickness of the vessel, $R_0 = (a+b)/2$ is the average radius, and $D_0 = 2R_0$ is the average diameter of the cylindrical vessel.

A comparison of the results with those from the known 2-D pressure vessel problem is also presented in Table 1 for a better understanding of the influence of the vessels' end supports on the displacement and stresses. The radial displacement and stresses from a 2-D plane-stress static solution for thick-walled pressure vessels subjected to the uniform pressure P_0 are given as (Sadd, 2009):

$$\begin{Bmatrix}\sigma_\theta^{2D}\\ \sigma_r^{2D}\end{Bmatrix} = \frac{1 \pm (b/r)^2}{(b/a)^2 - 1}P_0 \quad (36a,b)$$

$$u_r^{2D} = \frac{1}{E}\int(\sigma_r^{2D} - \nu\sigma_\theta^{2D})dr = \frac{r\left[1-\nu+(1+\nu)(b/r)^2\right]}{(b/a)^2-1}\frac{P_0}{E} \quad (36c)$$

It should be clarified that since both ends of the cylinder are open in the present 3-D problem, the influence of the tensile stresses due to the internal pressure acting on the vessel's end plates is not considered on σ_z, and therefore, only the 3-D effects of the ending supports are captured. This implies that a 2-D plane-stress solution is comparable with the present solution. Obviously, the mentioned closed-end effects can be considered by superposing a tensile rod-type of solution of the cylinder to the present 3-D solution.

It can be seen from Table 1 that by increasing the length of the cylinders, the radial displacements asymptotically approach those of a 2-D plane stress problem. Furthermore, while the normal axial stress in a long cylinder vanishes, the magnitude of that component of stress increases on the cylinders' inner and outer surfaces when the length of the cylinder decreases. Obviously, that is due to the bending of the cylinder's shell caused by the end supports. Therefore, the inner surface possesses normal compressive stress whereas the outer surface is in tension.

3.1.2. Example 2 – thick-walled cylindrical vessels, radially loaded by a liquid pressure

Treating a non-axisymmetric example based on the developed solution approach, assume a thick-walled cylindrical vessel, fully filled with a liquid, as shown in Fig. 2. The non-uniform internal pressure load is then given as

$$p_i = \rho g a(1+\cos\theta), \quad -\pi \le \theta \le \pi \quad (37)$$

where ρ is the density of the liquid, g the gravitational acceleration, and a the internal radius of the thick-walled cylinder. Using Eq. (30), the coefficients of the load series are determined as

$$P_{m0} = P_{m1} = \frac{2\rho g a}{\pi m}[1-(-1)^m],$$
$$P_{mn} = 0, \quad (n \ge 2) \quad (38)$$

and hence, the corresponding load in the form of the double Fourier series is represented as

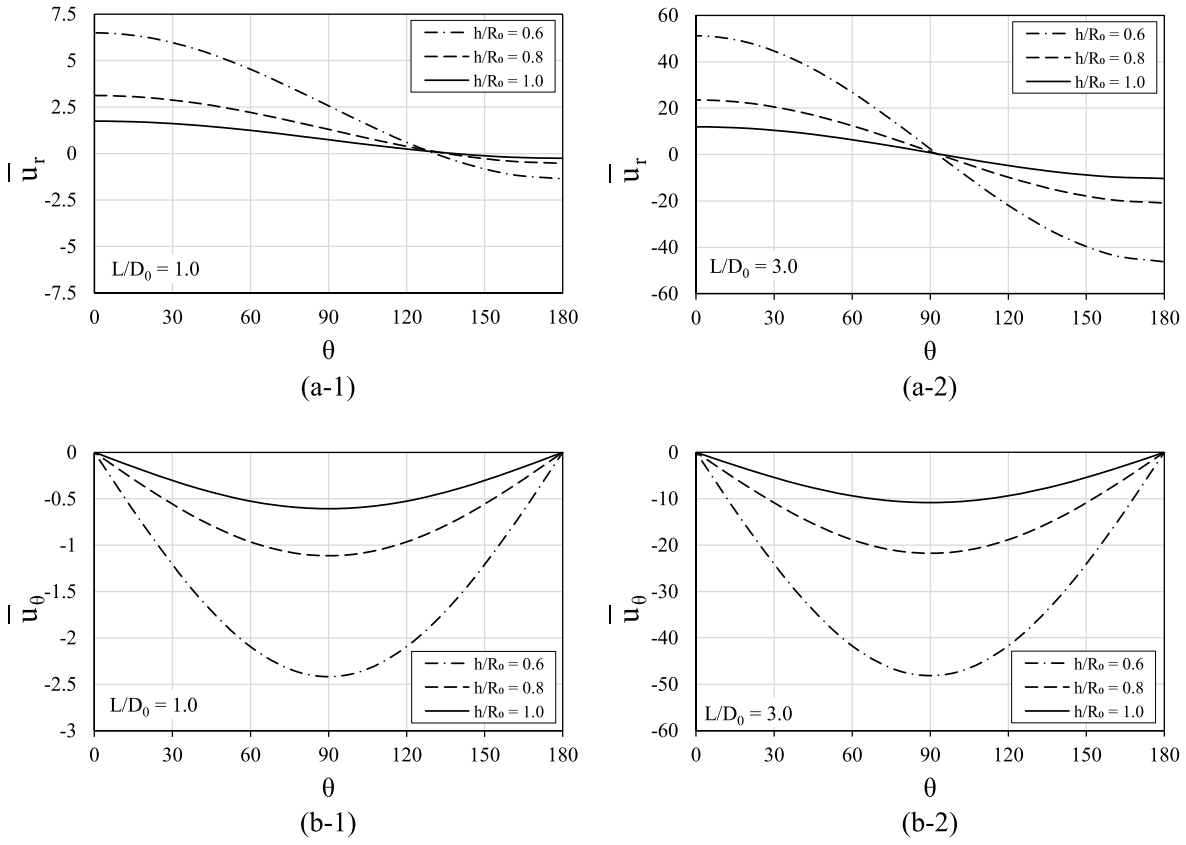

Fig. 3. Variation of the dimensionless displacement components along the tangential direction in thick-walled cylinders with different values of thickness-to-average radius ratio (h/R_0), radially loaded by fully filled liquid pressure: (a-1,2) radial displacement $\bar{u}_r|_{r=a,z=L/2}$ for the length-to-average diameter ratio $L/D_0 = 1$ and 3, respectively; (b-1,2) tangential displacement $\bar{u}_\theta|_{r=a,z=L/2}$ for $L/D_0 = 1$ and 3, respectively.

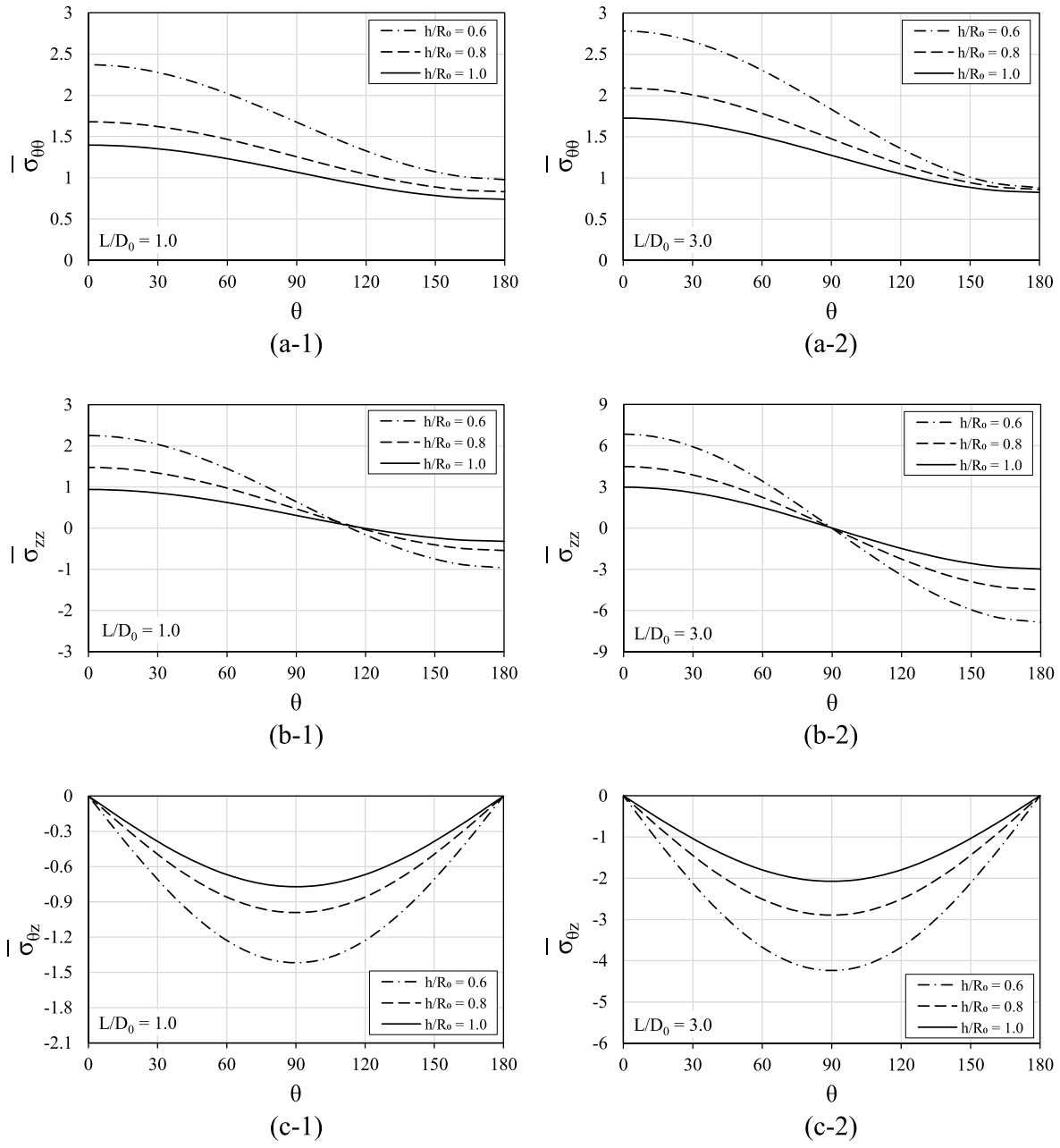

Fig. 4. Variation of the dimensionless stress components along the tangential direction in thick-walled cylinders with different values of thickness-to-average radius ratio (h/R_0), radially loaded by fully filled liquid pressure: (a-1,2) circumferential $\bar{\sigma}_{\theta\theta}|_{r=a,z=L/2}$ for the length-to-average diameter ratio $L/D_0 = 1$ and 3, respectively; (b-1,2) longitudinal stress $\bar{\sigma}_{zz}|_{r=b,z=L/2}$ for $L/D_0 = 1$ and 3, respectively; (c-1,2) shear stress $\bar{\sigma}_{\theta z}|_{r=a,z=0}$ for $L/D_0 = 1$ and 3, respectively.

$$p_i(\theta,z) = \frac{4}{\pi}\rho g a \sum_{m=1,3,\ldots}^{\infty}\sum_{n=0}^{1}\frac{1}{m}\cos n\theta \sin \alpha_m z \tag{39}$$

where, obviously $\alpha_m = m\pi/L$.

Based on the load series definition by Eq. (39), we set the tangential half-wave number $n = 0$ and 1 into Eq. (20a,b) and obtain the displacement component u_z and the rotation function $\omega_{r\theta}$ in the form

$$\begin{aligned} u_z &= \sum_{m=1,3,\ldots}^{\infty}[U_{z\,m0}(r) + U_{z\,m1}(r)\cos\theta]\cos\alpha_m z \\ \omega_{r\theta} &= \sum_{m=1,3,\ldots}^{\infty}\Omega_{r\theta\,m1}(r)\sin\theta\sin\alpha_m z \end{aligned} \tag{40}$$

in which the series coefficients functions are given from Eq. (23), accordingly. Next, the displacement components u_r and u_θ are obtained, using Eq. (24a,b), as follows

$$\begin{aligned} u_r &= \sum_{m=1,3,\ldots}^{\infty}[U_{r\,m0}(r) + U_{r\,m1}(r)\cos\theta]\sin\alpha_m z \\ u_\theta &= \sum_{m=1,3,\ldots}^{\infty}U_{\theta\,m1}(r)\sin\theta\sin\alpha_m z \end{aligned} \tag{41}$$

Obviously, the series coefficient functions $U_{r\,m0}$, $U_{r\,m1}$ and $U_{\theta\,m1}$ are given from Eq. (25a,b).

In the above equations, c_{1m0} through c_{4m0}, as well as c_{1m1} through c_{6m1} are totally ten coefficients in terms of m that are determined from satisfying two set of boundary equations as follows:

$$S^{rz}_{m0}(a) = S^{rz}_{m0}(b) = S^{rr}_{m0}(b) = 0, \quad S^{rr}_{m0}(a) = -\frac{4\rho g a}{\pi m} \tag{42a}$$

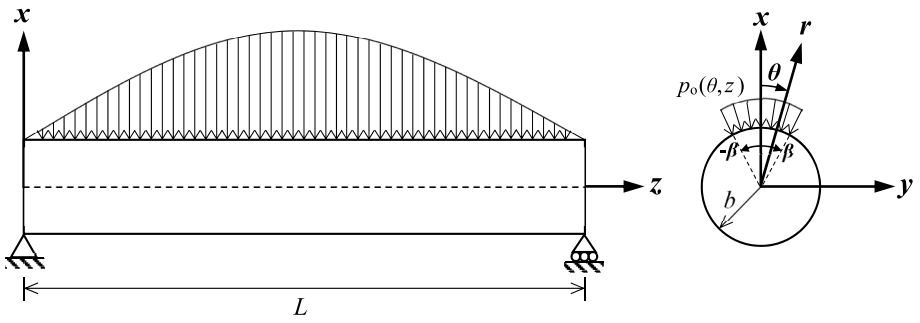

Fig. 5. A simply-supported beam with solid circular cross-section subjected to a sinusoidal distributed load.

$$S^{r\theta}_{m1}(a)=S^{r\theta}_{m1}(b)=S^{rz}_{m1}(a)=S^{rz}_{m1}(b)=S^{rr}_{m1}(b)=0,\quad S^{rr}_{m1}(a)=-\frac{4\rho ga}{\pi m} \tag{42b}$$

where $S^{x_i x_j}_{mn}(r)$ are the radial function coefficients in the series of the stress components as

$$\begin{aligned}\sigma_{rr}&=\sum_{m=1,3,\ldots}^{\infty}\left[S^{rr}_{m0}(r)+S^{rr}_{m1}(r)\cos\theta\right]\sin\alpha_m z\\ \sigma_{rz}&=\sum_{m=1,3,\ldots}^{\infty}\left[S^{rz}_{m0}(r)+S^{rz}_{m1}(r)\cos\theta\right]\cos\alpha_m z\\ \sigma_{r\theta}&=\sum_{m=1,3,\ldots}^{\infty}S^{r\theta}_{m1}(r)\sin\theta\sin\alpha_m z\end{aligned} \tag{43}$$

For generality of the results and convenience, the following dimensionless displacement and stress parameters are defined for this problem:

$$\bar{u}_i=\frac{Eu_i}{\rho gah},\quad \bar{\sigma}_{ij}=\frac{\sigma_{ij}}{\rho ga},\quad i,j\in\{r,\theta,z\} \tag{44}$$

where, as introduced previously, $R_0=(a+b)/2$ is the average radius of the thick-walled cylinder, $D_0=2R_0$ is the average diameter, and $h=(b-a)$ is the thickness of the cylinder. Also, a and b are the inner and outer radii of the cylinder, respectively.

In Fig. 3, variations of the displacement components along the tangential direction are depicted in radially-loaded thick-walled cylinders equivalent to a fully-filled liquid tank, for different values for thickness-to-average radius ratio (h/R_0). Moreover, variations of different stress components are illustrated in Fig. 4. All the results are presented for two different values of the cylinder's length-to-average diameter ratio (L/D_0), corresponding to a short and relatively long cylinders.

It can be seen from Figs. 3a–1,2 that, as expected, the magnitude of the dimensionless radial displacement at the center of the cylindrical vessel increases for the longer or thinner cylinders. It can also be concluded that the effect of the end supports is less influential on the maximum deflection of the liquid-filled cylinders at the middle as the magnitude of the deflection at the top and bottom of them are almost similar. However, the effect of the supports for the shorter cylinders is dominant as the supports causes a stretch of the upper part of the cylinders and consequently the maximum deflection at the top surface becomes lower than that at the bottom. The same conclusion may be drawn from Figs. 4b–1,2 for the longitudinal normal stress components. Clearly, the effect of stretching from the supports on the upper part of the cylindrical vessels is less important, and far from the supports in a long cylinder subjected to the weight load of the filled liquid, a quasi-pure bending action can be seen.

From Fig. 4, it can also be concluded that, while decreasing the thickness of the vessel wall or its length results in a significant increase of the normal axial and shear stresses, the hoop stress is not severely affected by the mentions geometrical changes.

3.1.3. Example 3 – beam with solid circular cross-section under a transverse load

Consider a simply-supported short beam having a solid circular section, subjected to a half-sine distributed transverse load along the longitudinal direction, as shown in Fig. 5. The load is circumferentially distributed on the perimeter with the tangential angle $-\beta\le\theta\le\beta$, acting in radial direction (see Fig. 5).

Based on the classical strength of materials, a half-sine distributed transverse load acting on a beam, q, is defined in the form of force per unit length along the longitudinal direction of the beam.; i.e.,

$$q(z)=q_0\sin\frac{\pi}{L}z \tag{45}$$

Here, the problem is treated based on the 3-D elasticity as a beam subjected to a distributed pressure load, as described earlier, in the form:

$$p(\theta,z)=\begin{cases}0, & -\pi\le\theta\le-\beta\\ p_0\sin(\pi z/L), & -\beta\le\theta\le\beta\\ 0, & \beta\le\theta\le\pi\end{cases} \tag{46}$$

Obviously, the distributed load per unit area $p(\theta,z)$ can be correlated to that per unit length $q(z)$ based on the 2-D strength of materials hypothesis, as

$$q(z)\equiv\int_{-\pi}^{\pi}p(\theta,z)b\cos\theta\,\mathrm{d}\theta \tag{47}$$

where b is the radius of the cross-section (see Fig. 5). Eq. (47) implies that,

$$p_0=\frac{q_0}{2b\sin\beta} \tag{48}$$

The distributed load by Eq. (46) can be represented in the general form of a double Fourier series (29), in which the coefficients are obtained using Eq. (30) as

$$\begin{aligned}&P_{10}=\frac{\beta p_0}{\pi},\\ &P_{1n}=\frac{2p_0}{n\pi}\sin n\beta,\quad (n\ge1)\\ &P_{mn}=0,\quad (m\ge2)\end{aligned} \tag{49}$$

Thus, the load function is represented, using Eq. (48), in the form,

$$p(\theta,z)=\frac{q_0}{2\pi b\sin\beta}\left(\beta+2\sum_{n=1}^{\infty}\frac{1}{n}\sin n\beta\cos n\theta\right)\sin\frac{\pi}{L}z \tag{50}$$

Based on different terms of the load series (see Eqs. (49) and (50)), and considering the fact that the modified Bessel function of the second kind Kmust vanish from the solution to have a finite displacement at the center of the cross-section (i.e., at $r=0$), the solutions for the transverse displacement and rotation function from Eq. (20a,b) are determined as

$$u_z = \left(\sum_{n=0}^{\infty} U_{z\ 1n}(r)\cos n\theta\right)\cos\frac{\pi}{L}z \tag{51a}$$

$$\omega_{r\theta} = \left(\sum_{n=1}^{\infty} \Omega_{r\theta\ 1n}(r)\sin n\theta\right)\sin\frac{\pi}{L}z \tag{51b}$$

where Eq. (23a,b) give the coefficient functions:

$$U_{z\ 1n}(r) = c_{11n}I_n(\pi r/L) + c_{31n}rI_{n+1}(\pi r/L) \tag{52a}$$

$$\Omega_{r\theta\ 1n}(r) = c_{51n}I_n(\pi r/L) \tag{52b}$$

and consequently, other components of the displacement field are determined as follows,

$$u_r = \left(\sum_{n=0}^{\infty} U_{r\ 1n}(r)\cos n\theta\right)\sin\frac{\pi}{L}z \tag{53a}$$

$$u_\theta = \left(\sum_{n=1}^{\infty} U_{\theta\ 1n}(r)\sin n\theta\right)\sin\frac{\pi}{L}z \tag{53b}$$

in which

$$\begin{aligned}
U_{r\ 10} &= \frac{L}{\pi}\left[c_{110}I_0'(\pi r/L) - c_{310}\left(\frac{\eta+\mu}{\eta-\mu}I_1(\pi r/L) - rI_1'(\pi r/L)\right)\right],\\
U_{r\ 1n} &= \frac{L}{\pi}\left\{c_{11n}I_n'(\pi r/L) - c_{31n}\left[\frac{2\eta}{\eta-\mu}\left(1+\frac{n(n+1)}{(\pi r/L)^2}\right)-1\right]I_{n+1}(\pi r/L) - c_{31n}\left(\frac{\eta}{\eta-\mu}\frac{2n}{(\pi r/L)^2}-1\right)rI_{n+1}'(\pi r/L) + c_{51n}\frac{2n}{\pi r/L}I_n(\pi r/L)\right\}
\end{aligned} \tag{54a}$$

$$\begin{aligned}
U_{\theta\,1n} = &\\
&-\frac{L}{\pi}\left\{c_{11n}\frac{n}{r}I_n(\pi r/L) - nc_{31n}\left[\frac{2\eta}{\eta-\mu}\frac{I_n(\pi r/L)}{\pi r/L} - I_{n+1}(\pi r/L)\right] + c_{51n}\frac{2L}{\pi}I_n'(\pi r/L)\right\}
\end{aligned} \tag{54b}$$

In the above equations, the unknown coefficients c_{110} and c_{310}, as well as c_{11n}, c_{31n} and c_{51n} are to be determined from satisfaction of two set of boundary equations which results in the following independent set of algebraic equations:

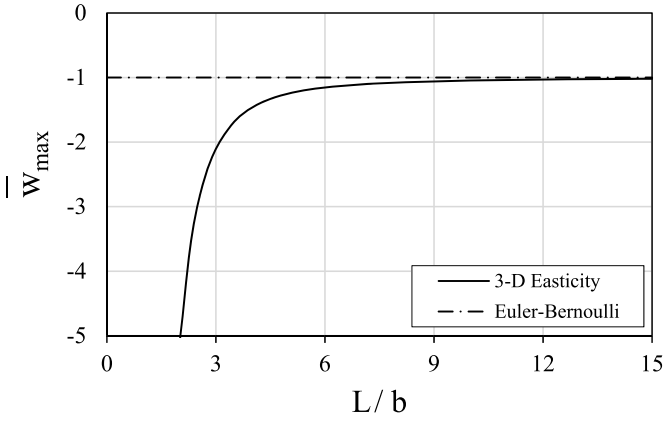

Fig. 6. Comparison of the dimensionless maximum deflection of simply-supported beams with solid circular cross-section subjected to half-sine distributed load, based on the 3-D solution and the classical Euler-Bernoulli theory.

$$S_{10}^{rz}(b) = 0, \quad S_{10}^{rr}(b) = -\frac{\beta p_0}{\pi} \quad \rightarrow c_{110},\ c_{310} \tag{55}$$

and

$$S_{1n}^{r\theta}(b) = S_{1n}^{rz}(b) = 0, \quad S_{1n}^{rr}(b) = -\frac{2p_0}{n\pi}\sin n\beta \quad \rightarrow c_{11n},\ c_{31n},\ c_{51n} \tag{56}$$

where $S_{mn}^{x_ix_j}(r)$ are the radial function coefficients in the series of the stress components as,

$$\begin{aligned}
\sigma_{rr}(r,\theta,z) &= \left(\sum_{n=0}^{\infty} S_{1n}^{rr}(r)\cos n\theta\right)\sin\frac{\pi}{L}z\\
\sigma_{rz}(r,\theta,z) &= \left(\sum_{n=0}^{\infty} S_{1n}^{rz}(r)\cos n\theta\right)\cos\frac{\pi}{L}z\\
\sigma_{r\theta}(r,\theta,z) &= \left(\sum_{n=1}^{\infty} S_{1n}^{r\theta}(r)\sin n\theta\right)\sin\frac{\pi}{L}z
\end{aligned} \tag{57}$$

To have a better understanding and insight about how the displacements and stresses in a stocky beam deviate from those ideally captured based of the classical Euler-Bernoulli hypothesis, the comparative results of this example are presented in the form of the following dimensionless parameters:

$$\begin{aligned}
\overline{w}_{\max} &= \frac{\pi^5 Eb^4}{4q_0L^4}u_r(b,0,L/2)\\
\overline{\sigma}_{zz} &= \frac{\pi^3 b^3}{4q_0L^2}\sigma_{zz}(r,\theta,L/2), \quad \theta = \text{either 0 or } \pi\\
\overline{\sigma}_{xz} &= \frac{3\pi^2 b^2}{4q_0L}\sigma_{rz}(r,\theta,L), \quad \theta = \text{either 0 or } \pi
\end{aligned} \tag{58}$$

In Fig. 6, variation of the normalized maximum deflection of simply-supported beams versus the length-to-cross-section radius parameter from the present 3-D elasticity solution is depicted in comparison with that based on of the classical Euler-Bernoulli beam theory.

It can be observed that for sufficiently large beams, there is a very good agreement between the predicted deflections based on the two theories. As it is expected, the classical Euler-Bernoulli theory underpredicts the beam deflection compared to the 3-D elasticity theory, especially for stocky beams. This is obviously due to the fact that the classical beam theory neglects the effect of shear deformations which exhibits a greater impact on the deflection for smaller values of the beam length-to depth parameter; i.e., the shorter beams.

Variations of the dimensionless normal bending stress, $\overline{\sigma}_{zz}$, and the out-of-plane shear stress, $\overline{\sigma}_{xz}$, through the depth of the beam are respectively illustrated in Figs. 7 and 8, for three different values of the beam length-to-cross-section radius rati, together with a comparison with those based on the simplest Euler-Bernoulli beam theory. While the classical beam theory yields a linear and parabolic distribution through the beam depth, respectively for the normal bending stress and the shear stress, the 3-D stresses deviate from those idealized stress distributions when the beam length-to-radius in depth parameter, L/b, decreases.

Variation of the curves in Figs. 7 and 8 reveals the fact that the

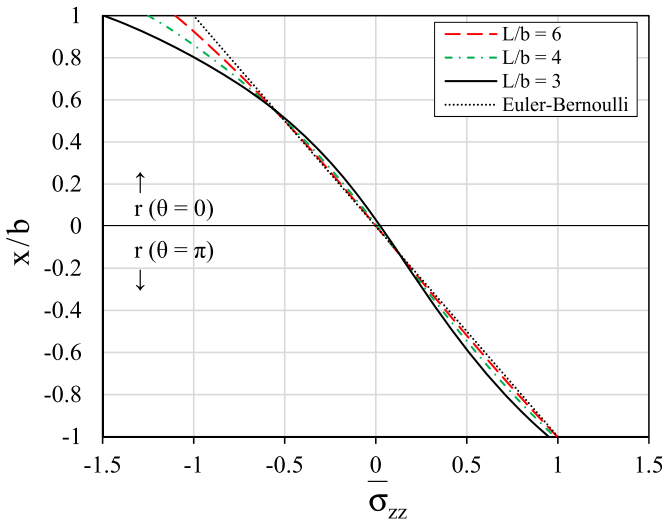

Fig. 7. Through-depth distribution of the dimensionless normal bending stress for different values of beam length-to-cross-section radius ratio, and comparison with the classical Euler-Bernoulli beam theory.

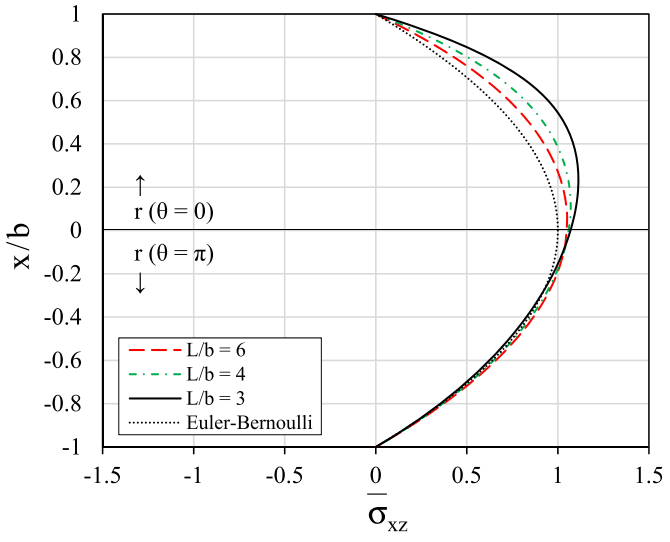

Fig. 8. Through-depth distribution of the dimensionless out-of-plane shear stress for different values of beam length-to-cross-section radius ratio, and comparison with the classical Euler-Bernoulli beam theory.

concept of the neutral line/plane and the symmetric/antisymmetric distribution of the stresses through the depth is not valid for the short beams. Obviously, the intensity of the maximum compressive stress at the outermost upper surface of the beam is larger than what predicted by the classical theories due the direct impact of the applied transverse load. In a similar logic, the location of the maximum shear stress is shifted upwards closer to the region where the external load is applied. It can also be deduced from Fig. 7 that by decreasing the beam length-to-depth parameter, not only the neutral plane is not coincident with the location of the center of area, also the nonlinearity in the in-depth distribution of the normal stress increases.

3.2. Exact elasto-dynamic solutions

Consider a thick-walled hollow circular cylinder of inner and outer radii a and b, respectively, and length L, simply supported at both ends. As the basis of several elasto-dynamic problems, the three-dimensional free vibration problem is treated in this subsection based on the introduced uncoupling solution approach to prove the validity and easiness of implementing the approach. A general exact analytical solution is presented to extract the 3-D natural frequencies and the corresponding mode-shapes of the mentioned thick-walled cylinders.

Using the method of separation of variables for a hollow closed circular cylinder having finite length, the displacement along the longitudinal direction, z, as well as the rotation component $\omega_{r\theta}$, can be described using the double Fourier series as

$$u_z(r,\theta,z,t)=\sum_{m=1}^{\infty}\sum_{n=0}^{\infty}U_{z\,mn}(r)e^{j\varpi_{mn}t}\cos n\theta\cos\alpha_m z \tag{59a}$$

$$\omega_{r\theta}(r,\theta,z,t)=\sum_{m=1}^{\infty}\sum_{n=1}^{\infty}\Omega_{r\theta\,mn}(r)e^{j\varpi_{mn}t}\sin n\theta\sin\alpha_m z,\quad j=\sqrt{-1} \tag{59b}$$

where $U_{z\,mn}(r)$ and $\Omega_{r\theta\,mn}(r)$ are two unknown functions of the radial variable, r, only; n is the number of half-waves superimposed to describe the deformed shape in the circumferential direction, and $\alpha_m=m\pi/L$ indicates the deformed shape of the cylinder along the longitudinal direction with m number of half-waves. Obviously, the trigonometric functions of θ and z in Eq. (59a,b) exactly satisfy the simply-supported end boundary conditions (see Eq. (21)) and the continuity of a closed cylinder in the hoop direction. Moreover, ϖ_{mn} indicates natural frequencies corresponding to the half-wave numbers m and n along the longitudinal and circumferential directions, respectively, and the variable t is the time. Apparently, corresponding to each m and n values, there are theoretically an infinite number of frequencies corresponding to different half-waves along the radial direction in 3-D vibrations.

Substituting Eq. (59a,b) into the uncoupled governing partial differential Eqs. (11) and (12), respectively, results in the following two independent ordinary differential equations:

$$\begin{aligned}&U^{(4)}_{z\,mn}(r)+\frac{2}{r}U'''_{z\,mn}(r)-\left[\frac{1}{r^2}\left(1+2n^2\right)+2\alpha_m^2-\frac{(\eta+\mu)\rho\varpi_{mn}^2}{\eta\mu}\right]U''_{z\,mn}(r)\\&+\frac{1}{r}\left[\frac{1}{r^2}\left(1+2n^2\right)-2\alpha_m^2+\frac{(\eta+\mu)\rho\varpi_{mn}^2}{\eta\mu}\right]U'_{z\,mn}(r)\\&+\left[\left(n^2-4\right)\frac{n^2}{r^4}+2\alpha_m^2\frac{n^2}{r^2}-\frac{(\eta+\mu)\rho\varpi_{mn}^2}{\eta\mu}\left(\alpha_m^2+\frac{n^2}{r^2}\right)+\frac{\rho^2\varpi_{mn}^4}{\eta\mu}+\alpha_m^4r^2\right]U_{z\,mn}(r)=0\end{aligned} \tag{60a}$$

$$\Omega''_{r\theta\,mn}+\frac{1}{r}\Omega'_{r\theta\,mn}-\frac{1}{r^2}\left[n^2+\left(\alpha_m^2-\frac{\rho\varpi_{mn}^2}{\mu}\right)r^2\right]\Omega_{r\theta\,mn}=0 \tag{60b}$$

It is easy to show that the exact solutions of the ordinary differential Eq. (60a,b) can be expressed in the form:

$$U_{z\,mn}(r)=c_{1mn}I_n(\lambda_{1\,mn}r)+c_{2mn}K_n(\lambda_{1\,mn}r)+c_{3mn}I_n(\lambda_{2\,mn}r)+c_{4mn}K_n(\lambda_{2\,mn}r) \tag{61a}$$

$$\Omega_{r\theta\,mn}(r)=c_{5mn}I_n(\lambda_{2\,mn}r)+c_{6mn}K_n(\lambda_{2\,mn}r) \tag{61b}$$

where

$$\lambda_{1\,mn}=\sqrt{\alpha_m^2-\frac{\rho\varpi_{mn}^2}{\eta}} \tag{62a}$$

$$\lambda_{2\,mn}=\sqrt{\alpha_m^2-\frac{\rho\varpi_{mn}^2}{\mu}} \tag{62b}$$

Also c_{1mn} through c_{6mn} are six coefficients to be determined from satisfaction of the boundary conditions at the internal and external surfaces of the thick-walled cylinder. Also, substituting Eq. (59a,b) into Eq. (18a,b) and integrating three times with respect to the variable z, other components of the displacement field are obtained as

$$u_r(r,\theta,z,t)=\sum_{m=1}^{\infty}\sum_{n=0}^{\infty}U_{r\ mn}(r)e^{j\varpi_{mn}t}\cos n\theta\sin\alpha_m z \tag{63a}$$

$$u_\theta(r,\theta,z,t)=\sum_{m=1}^{\infty}\sum_{n=1}^{\infty}U_{\theta\ mn}(r)e^{j\varpi_{mn}t}\sin n\theta\sin\alpha_m z \tag{63b}$$

in which

$$\begin{aligned}U_{r\ mn}(r)=&\gamma_{1\ mn}\left[c_{1mn}I_n'(\lambda_{1\ mn}r)+c_{2mn}K_n'(\lambda_{1\ mn}r)\right]+\gamma_{2\ mn}\left[c_{3mn}I_n'(\lambda_{2\ mn}r)+c_{4mn}K_n'(\lambda_{2\ m}r)\right]\\&+\frac{2n}{\lambda_{2\ mn}^2}\frac{1}{r}\left[c_{5mn}I_n(\lambda_{2\ mn}r)+c_{6mn}K_n(\lambda_{2\ mn}r)\right]\end{aligned} \tag{64a}$$

$$\begin{aligned}U_{\theta\ mn}(r)=&-\frac{n}{r}\gamma_{1\ mn}\left[c_{1mn}I_n(\lambda_{1\ mn}r)+c_{2mn}K_n(\lambda_{1\ mn}r)\right]-\frac{n}{r}\gamma_{2\ mn}\left[c_{3mn}I_n(\lambda_{2\ mn}r)+c_{4mn}K_n(\lambda_{2\ mn}r)\right]\\&-\frac{2}{\lambda_{2\ mn}^2}\left[c_{5mn}I_n'(\lambda_{2\ mn}r)+c_{6mn}K_n'(\lambda_{2\ mn}r)\right]\end{aligned} \tag{64b}$$

where the coefficients $\gamma_{1\ mn}$ and $\gamma_{2\ mn}$ are given as

$$\begin{Bmatrix}\gamma_{1\ mn}\\ \gamma_{2\ mn}\end{Bmatrix}=\frac{1}{\alpha_m\lambda_{2\ mn}^2(\eta-\mu)}\left[(2\eta-\mu)\alpha_m^2-\begin{Bmatrix}\lambda_{1\ mn}^2\\ \lambda_{2\ mn}^2\end{Bmatrix}-\frac{\eta}{\mu}\rho\varpi_{mn}^2\right] \tag{65}$$

The stress components are also determined by substituting the obtained exact closed-form equations for the displacements (i.e., Eqs. (59a) and (61a) for u_z, together with Eqs. (63)–(65) for u_r and u_θ) into the linear strain-displacement relations in the cylindrical coordinates (Eq. (26)) and next replacing the results into the constitutive Hooke's law for the linear elastic isotropic material, represented by Eq. (27).

As mentioned earlier, the displacement field of Eq. (59) satisfies the simply supported boundary conditions as well as the continuity of a hollow circular cylinder. Next, the remaining boundary conditions related to the free stress surfaces need to be satisfied:

$$\begin{aligned}&\sigma_{r\theta}|_{r=a}=\sigma_{r\theta}|_{r=b}=0\\&\sigma_{rz}|_{r=a}=\sigma_{rz}|_{r=b}=0\\&\sigma_{rr}|_{r=a}=\sigma_{rr}|_{r=b}=0\end{aligned} \tag{66}$$

In the following, some practical examples are analytically solved based on the presented solution approach, and the numerical results are presented in comparison with FE simulation.

Table 2
First five eigen-frequency parameters (ϖ^*) and corresponding mode-shapes of solid cylinders, and comparison with the 3-D FE results for different values of length-to-cross-section radius ratio.

L/b	Frequencies & mode-shapes	Mode sequences				
		1st	2nd	3rd	4th	5th
2.0	Present	$0.7139^{1,1*}$	$1.4428^{1,0}$	$1.5101^{1,2}$	$1.7076^{2,1}$	$1.7841^{1,1}$
	3-D FEM	0.7136 (0.04%)†	1.4420 (0.06%)	1.5082 (0.12%)	1.7060 (0.09%)	1.7810 (0.17%)
	Beam theory	1.2337 (72.8%)†	–	–	4.9348 (188%)	–
		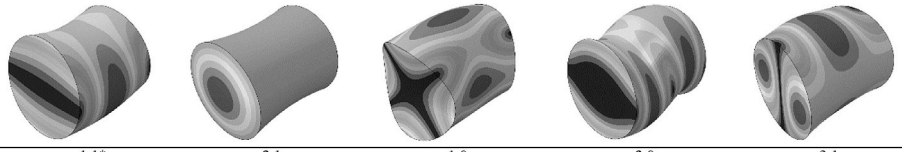				
4.0	Present	$0.2486^{1,1*}$	$0.7139^{2,1}$	$0.7734^{1,0}$	$0.9742^{2,0}$	$1.2118^{3,1}$
	3-D FEM	0.2482 (0.16%)	0.7136 (0.04%)	0.7733 (0.01%)	0.9730 (0.12%)	1.2111 (0.06%)
	Beam theory	0.3084 (24.1%)	1.2337 (72.8%)	–	–	2.7758 (129%)
		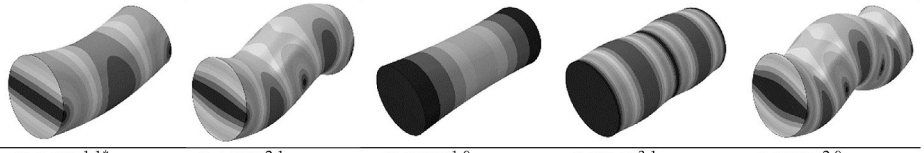				
10	Present	$0.0475^{1,1*}$	$0.1696^{2,1}$	$0.3135^{1,0}$	$0.3342^{3,1}$	$0.3897^{2,0}$
	3-D FEM	0.0471 (0.84%)	0.1692 (0.24%)	0.3134 (0.03%)	0.3337 (0.15%)	0.3880 (0.44%)
	Beam theory	0.0493 (3.79%)	0.1974 (16.4%)	–	0.4441 (32.9%)	–
		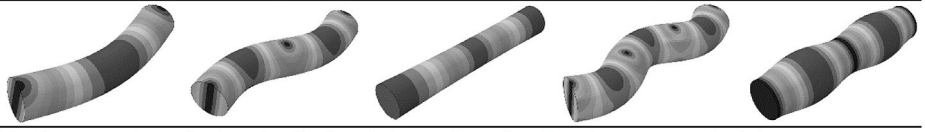				

* m,n (number of half-waves along the longitudinal and circumferential directions, respectively).
† Percentage difference with respect to the present exact 3-D results.

Table 3
First five eigen-frequency parameters (ϖ^*) and corresponding mode-shapes of thick-walled cylindrical shells, and comparison with the 3-D FE results for different values of the length-to-average diameter and the thickness-to-average radius parameters.

L/D_0	h/R_0	Frequencies & mode-shapes	Mode sequences 1st	2nd	3rd	4th	5th
1.0	0.2	Present	$0.4411^{1,2*}$	$0.5864^{1,3}$	$0.6143^{1,1}$	$0.9220^{1,4}$	$0.9656^{2,2}$
		FEM (3-D)	0.4395	0.5816	0.6139	0.9140	0.9620
		|%Diff|	0.36%	0.83%	0.07%	0.87%	0.37%
							
	0.4	Present	$0.6085^{1,2}$	$0.6487^{1,1}$	$0.9653^{1,3}$	$0.9982^{1,0}$	$1.2946^{2,1}$
		FEM (3-D)	0.6075	0.6484	0.9632	0.9976	1.2930
		|%Diff|	0.16%	0.05%	0.21%	0.06%	0.12%
			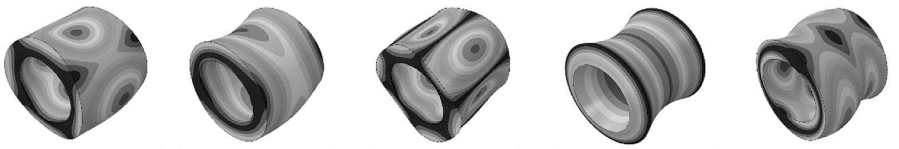				
2.0	0.2	Present	$0.2182^{1,2}$	$0.2714^{1,1}$	$0.4411^{2,2}$	$0.4671^{1,3}$	$0.5865^{2,3}$
		FEM (3-D)	0.2167	0.2714	0.4394	0.4630	0.5819
		|%Diff|	0.69%	0.02%	0.39%	0.88%	0.79%
							
	0.4	Present	$0.2774^{1,1}$	$0.3632^{1,2}$	$0.6086^{2,2}$	$0.6487^{2,1}$	$0.7447^{1,0}$
		FEM (3-D)	0.2774	0.3624	0.6075	0.6487	0.7447
		|%Diff|	0.02%	0.22%	0.18%	0.01%	0.00%
			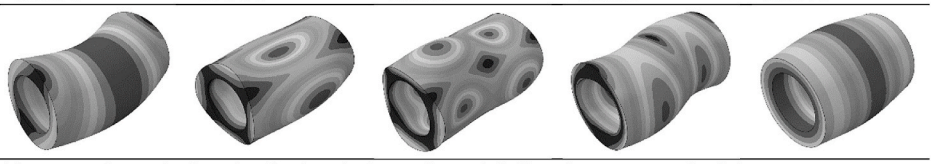				

* m,n (number of half-waves along the longitudinal and circumferential directions, respectively).

3.2.1. Example 4 – free vibrations of solid cylinders

Assume an isotropic elastic solid cylinder of finite length L, simply-supported at both ends and vibrating freely with a 3-D natural frequency ϖ. To extract the eigen-frequencies ϖ and corresponding eigen-mode-shape functions, a non-trivial solution must be conducted from the set of the remaining boundary conditions (i.e., the stress-free conditions at the perimeter surface of the solid cylinder):

$$\sigma_{rr}|_{r=b} = \sigma_{r\theta}|_{r=b} = \sigma_{rz}|_{r=b} = 0 \tag{67}$$

where b is the radius of the solid cylinder's cross-section. To have a finite value for the longitudinal displacement u_z and rotation $\omega_{r\theta}$ at any point on the center line of the cylinder, the modified Bessel function of second kind, K_n, must vanish from the solutions (61a,b). Therefore, the longitudinal displacement u_z and the rotation $\omega_{r\theta}$ are presented in a simplified form as

$$u_z(r,\theta,z,t) = \sum_{m=1}^{\infty}\sum_{n=0}^{\infty}[c_{1mn}I_n(\lambda_{1\ mn}r) + c_{3mn}I_n(\lambda_{2\ mn}r)]e^{i\varpi_{mn}t}\cos n\theta\cos\alpha_m z \tag{68a}$$

$$\omega_{r\theta}(r,\theta,z,t) = \sum_{m=1}^{\infty}\sum_{n=1}^{\infty}c_{5mn}I_n(\lambda_{2\ mn}r)e^{i\varpi_{mn}t}\sin n\theta\sin\alpha_m z \tag{68b}$$

and consequently, the other components of the displacement field are given as

$$u_r = \sum_{m=1}^{\infty}\sum_{n=0}^{\infty}\left[c_{1mn}\gamma_{1\ mn}I_n'(\lambda_{1\ mn}r) + c_{3mn}\gamma_{2\ mn}I_n'(\lambda_{2\ mn}r) + c_{5mn}\frac{2n}{\lambda_{2\ mn}^2}\frac{1}{r}I_n(\lambda_{2\ mn}r)\right]e^{j\varpi_{mn}t}\cos n\theta \sin \alpha_m z \tag{69a}$$

$$u_\theta = -\sum_{m=1}^{\infty}\sum_{n=1}^{\infty}\frac{n}{r}\left[c_{1mn}\gamma_{1\ mn}I_n(\lambda_{1\ mn}r) + c_{3mn}\gamma_{2\ mn}I_n(\lambda_{2\ mn}r) + c_{5mn}\frac{2r}{n\lambda_{2\ mn}^2}I_n'(\lambda_{2\ mn}r)\right]e^{j\varpi_{mn}t}\sin n\theta.\sin \alpha_m z \tag{69b}$$

The normal stress σ_{rr} and the shear stresses $\sigma_{r\theta}$ and σ_{rz} are determined by substitution of Eqs. (68a) and (69a,b) into the strain-displacement relations (26) first, and next the results into the constitutive Hooke's law (27). Satisfying the stress-free surface conditions (67) leads to a set of three algebraic equations, in terms of the three coefficients c_{1mn}, c_{3mn} and c_{5mn}. Setting the determinant of the coefficient matrix of the equations equal to zero, an exact algebraic characteristic equation in terms of the half-wave numbers m and n are obtained. The roots of the characteristic equations determine the 3-D natural frequencies.

To demonstrate the validity of the presented solution approach for elasto-dynamic problems, the first five natural frequencies of solid cylinders are extracted and given together with their corresponding mode-shapes in Table 2, in comparison with corresponding results obtained from 3-D finite element analyses (FEA) using Abaqus software. For the sake of generality of the numerical results, a dimensionless frequency parameter is defined as

$$\varpi^* = \varpi R\sqrt{\rho/E} \tag{70}$$

where for the solid cylinder $R = b$ is the radius of cylinders' cross-section. The results are presented for three different values of the length-to-cross-section radius ratio: L/b = 2, 4 and 10, equivalent to short/stocky, moderately long and long slender solid cylinders. It can be observed from Table 2 that there is an excellent agreement between the results of the two approaches, confirming high accuracy and reliability of the proposed uncoupling solution approach for the 3-D elasto-dynamic problems in the curvilinear cylindrical coordinates. Moreover, a comparison of natural frequencies of flexural modes based on the Euler-Bernoulli beam equation as well as their difference percentage with respect to the 3-D solutions are presented. Obviously, the number of beam-type of flexural modes within the first five fundamental modes increases for slenderer/longer beams and, as it is seen from Table 2, discrepancy between the relevant frequency parameters decreases.

3.2.2. Example 5 – free vibration of thick-walled circular cylindrical shells

Similar to the previous example for the free vibration of solid cylinders, a non-trivial solution through satisfaction of the remaining boundary conditions will result in a characteristic equation having the natural frequencies as the roots. For a thick-walled circular cylindrical shell, applying the stress-free conditions at the inner and outer surfaces ($r = a, b$) yields a set of six algebraic equations (see Eq. (66)). Setting the determinant of the coefficients matrix equal to zero leads to determining eigen-frequencies and corresponding eigen-mode-shape functions.

In Table 3, the first five lowest frequencies and mode-shapes of the hollow thick-walled circular cylinders are presented and compared with corresponding results obtained from finite element modelling using 3-D solid elements in Abaqus software. The results are given in the form of dimensionless frequency parameter, presented by Eq. (70), in which R is set as the average radius of the shell thickness: $R = R_0 = (a + b)/2$. To verify the validity and accuracy of the obtained analytical solution based on the established uncoupling elasticity approach, the frequency parameter values and the mode shapes are provided, in comparison with the 3-D FE results, for two different values of the shell thickness-to-average radius ratio parameter: $h/R_0 = 0.2$ and 0.4, equivalent to moderately thick and thick shells. Moreover, two different values of the cylindrical shells length-to-average cross-section diameter (L/D_0) are considered. It is evident from the results of Table 3 that there exists an excellent agreement between the results of the present approach and those of the 3-D FE simulations, confirming the correctness and validity of the established 3-D elasto-dynamic approach.

4. Conclusions

In this paper, an exact representation of the three-dimensional elasticity equations of motion in the curvilinear cylindrical coordinate system was developed in an uncoupling form, without introducing any potential function or physically meaningless auxiliary parameter. An efficient straightforward flow of solution procedure was shown that need to be followed to gain exact 3-D solutions for both category of elasto-static and elasto-dynamic problems in the curvilinear cylindrical coordinate system. Validity and correctness of the approach was demonstrated through some analytical solutions for a number of classical problems within the area of solid and structural mechanics. The presented approach was shown to facilitate obtaining elasticity solutions, due to being on the basis of some independent uncoupled governing equations. Unlike most existing decomposition representations, it was shown that the governing equations of the new representation need to be directly solved in terms of some standard displacement and rotation components instead of some new physically-meaningless potentials. Needless to mention, this enables implementing solutions according to semi-inverse method using the introduced representation. The efficiency of the present approach was demonstrated through exact analytical solutions for some classical solid and hollow thick-walled cylinder problems.

Authorship contributions

Seyed Rasoul Atashipour: Conception and design of study, Acquisition of data, Analysis and/or interpretation of data, Drafting the manuscript, Revising the manuscript critically for important intellectual content, Approval of the version of the manuscript to be published, Zahra Mohammadi: Acquisition of data, Revising the manuscript critically for important intellectual content, Approval of the version of the manuscript to be published, Peter D. Folkow: Conception and design of study, Revising the manuscript critically for important intellectual content, Approval of the version of the manuscript to be published.

Declaration of competing interest

The authors declare that they have no known competing financial interests or personal relationships that could have appeared to influence the work reported in this paper.

References

Armenakas, A.E., Gazis, D.C., Hermann, G., 1969. Free Vibration of Circular Cylindrical Shells. Pergamon Press, Oxford, UK.

Atashipour, S.R., Saidi, A.R., Jomehzadeh, E., 2010. On the boundary layer phenomenon in bending of thick annular sector plates using third-order shear deformation theory. Acta Mech. 211, 89–99. https://doi.org/10.1007/s00707-009-0214-z.

Chou, P.C., Pagano, N.J., 2013. Elasticity: Tensor, Dyadic, and Engineering Approaches. courier corporation.

Chu, P., Li, X.-F., Wu, J., Lee, K., 2015. Two-dimensional elasticity solution of elastic strips and beams made of functionally graded materials under tension and bending. Acta Mech. 226, 2235–2253. https://doi.org/10.1007/s00707-014-1294-y.

Ecsedi, I., 2013. Some analytical solutions for Saint-Venant torsion of non-homogeneous anisotropic cylindrical bars. Mech. Res. Commun. 52, 95–100. https://doi.org/10.1016/j.mechrescom.2013.07.001.

Ecsedi, I., 2009. Some analytical solutions for Saint-Venant torsion of non-homogeneous cylindrical bars. Eur. J. Mech. - ASolids 28, 985–990. https://doi.org/10.1016/j.euromechsol.2009.03.010.

Ecsedi, I., Baksa, A., 2010. Prandtl's formulation for the Saint-Venant's torsion of homogeneous piezoelectric beams. Int. J. Solid Struct. 47, 3076–3083. https://doi.org/10.1016/j.ijsolstr.2010.07.007.

England, A.H., 2006. Bending solutions for inhomogeneous and laminated elastic plates. J. Elasticity 82, 129–173. https://doi.org/10.1007/s10659-005-9029-x.

Eskandari-Ghadi, M., 2005. A complete solution of the wave equations for transversely isotropic media. J. Elasticity 81, 1–19. https://doi.org/10.1007/s10659-005-9000-x.

Galerkin, B., 1930. Contribution á la solution générale du problème de la théorie de l'élasticité dans le cas de trios dimensions. Comptes Rendus 190, 1047.

Gazis, D.C., 1958. Exact analysis of the plane-strain vibrations of thick-walled hollow cylinders. J. Acoust. Soc. Am. 30, 786–794. https://doi.org/10.1121/1.1909761.

Hosseini Hashemi, Sh, Atashipour, S.R., Fadaee, M., 2012. An exact analytical approach for in-plane and out-of-plane free vibration analysis of thick laminated transversely isotropic plates. Arch. Appl. Mech. 82, 677–698. https://doi.org/10.1007/s00419-011-0583-3.

Hosseini-Hashemi, S., Arsanjani, M., 2005. Exact characteristic equations for some of classical boundary conditions of vibrating moderately thick rectangular plates. Int. J. Solid Struct. 42, 819–853. https://doi.org/10.1016/j.ijsolstr.2004.06.063.

Hosseini-Hashemi, Sh, Atashipour, S.R., Fadaee, M., Girhammar, U.A., 2012. An exact closed-form procedure for free vibration analysis of laminated spherical shell panels based on Sanders theory. Arch. Appl. Mech. 82, 985–1002. https://doi.org/10.1007/s00419-011-0606-0.

Hu, H.-C., 1953. On the three-dimensional problems of the theory of elasticity of a transversely isotropic body. Sci. Sin. 2, 145–151. https://doi.org/10.1360/ya1953-2-2-145.

Hutchinson, J.R., 1980. Vibrations of solid cylinders. J. Appl. Mech. 47, 901–907. https://doi.org/10.1115/1.3153811.

Jomehzadeh, E., Saidi, A.R., 2009. Analytical solution for free vibration of transversely isotropic sector plates using a boundary layer function. Thin-Walled Struct. 47, 82–88. https://doi.org/10.1016/j.tws.2008.05.004.

Kaljevic, I., Saigal, S., Hopkins, D.A., 1994. Completed Beltrami-Michell formulation for analyzing radially symmetrical bodies. NASA TM 4593.

Kaprielian, P.V., Rogers, T.G., Spencer, A.J.M., 1988. Theory of laminated elastic plates I. Isotropic laminae. Philos. Trans. R. Soc. Lond. Ser. Math. Phys. Sci. 324, 565–594.

Kari, L., 2002. Axially symmetric modes in finite cylinders - the wave guide solution. Wave Motion 36, 169–184.

Lazar, M., Maugin, G.A., 2005. Nonsingular stress and strain fields of dislocations and disclinations in first strain gradient elasticity. Int. J. Eng. Sci. 43, 1157–1184. https://doi.org/10.1016/j.ijengsci.2005.01.006.

Lazar, M., Maugin, G.A., Aifantis, E.C., 2006. On a theory of nonlocal elasticity of bi-Helmholtz type and some applications. Int. J. Solid Struct. 43, 1404–1421. https://doi.org/10.1016/j.ijsolstr.2005.04.027.

Leissa, A.W., So, J., 1995. Accurate vibration frequencies of circular cylinders from three-dimensional analysis. J. Acoust. Soc. Am. 98, 2136–2141. https://doi.org/10.1121/1.414403.

Liew, K.M., Hung, K.C., 1995. Three-dimensional vibratory characteristics of solid cylinders and some remarks on simplified beam theories. Int. J. Solid Struct. 32, 3499–3513. https://doi.org/10.1016/0020-7683(95)00004-T.

Love, A.E.H., 1927. A Treatise on the Mathematical Theory of Elasticity. Cambridge University Press.

Michell, J.H., 1899. On the direct determination of stress in an elastic solid, with application to the theory of plates. Proc. Lond. Math. Soc. s1–31, 100–124. https://doi.org/10.1112/plms/s1-31.1.100.

Muskhelishvili, N.J., 1963. Some Basic Problems of the Mathematical Theory of Elasticity; Fundamental Equations, Plane Theory of Elasticity, Torsion, and Bending (P. Noordhoff, Groningen).

Neuber, H., 1934. Ein neuer Ansatz zur Lösung räumlicher Probleme der Elastizitätstheorie. Der Hohlkegel unter Einzellast als Beispiel 14, 203. https://doi.org/10.1002/ZAMM.19340140404.

Nosier, A., Yavari, A., Sarkani, S., 2001a. A study of the edge-zone equation of Mindlin-Reissner plate theory in bending of laminated rectangular plates. Acta Mech. 146, 227–238. https://doi.org/10.1007/BF01246734.

Nosier, A., Yavari, A., Sarkani, S., 2001b. On a boundary layer phenomenon in Mindlin-Reissner plate theory for laminated circular sector plates. Acta Mech. 151, 149–161. https://doi.org/10.1007/BF01246914.

Nowacki, W., 1954. The stress function in three-dimensional problems concerning an elastic body characterized by transverse isotropy. Bull. Acad. Pol. Sci. 2, 21–25.

Papkovich, P., 1932. An expression for a general integral of the equations of the theory of elasticity in terms of harmonic functions. Izvest Akad Nauk SSSR Ser Phys Math 1425–1435.

Peckhold, D., 1971. On the role of the Stokes-Helmholtz decomposition in the derivation of displacement potentials in classical elasticity. J. Elasticity 1, 171–174.

Plevako, V.P., 1971. On the theory of elasticity of inhomogeneous media. J. Appl. Math. Mech. 35, 806–813. https://doi.org/10.1016/0021-8928(71)90078-5.

Prandtl, L., 1903. Zur torsion von prismatischen stäben. Phys. Z. 4, 758–770.

Sadd, M.H., 2009. Elasticity: Theory, Applications and Numerics, second ed. Elsevier Butterworth-Heinemann.

Saidi, A.R., Atashipour, S.R., Jomehzadeh, E., 2009. Reformulation of Navier equations for solving three-dimensional elasticity problems with applications to thick plate analysis. Acta Mech. 208, 227–235. https://doi.org/10.1007/s00707-009-0147-6.

Shen, L., Wang, J., Lu, D., Chen, W., Yang, B., 2022. A series of elasticity solutions for flexural responses of functionally graded annular sector plates. Eng. Struct. 256, 114070. https://doi.org/10.1016/j.engstruct.2022.114070.

Teodorescu, P., 1964. One hundred years of investigations in the plane problem of the theory of elasticity. Appl. Mech. Rev. 17, 175–186.

Wang, M.Z., Wang, W., 1995. Completeness and nonuniqueness of general solutions of transversely isotropic elasticity. Int. J. Solids Struct. 32, 501–513. https://doi.org/10.1016/0020-7683(94)00114-C. Special topics in the theory of elastic: A volume in honour of Professor John Dundurs.

Yang, B., Ding, H.J., Chen, W.Q., 2012. Elasticity solutions for functionally graded rectangular plates with two opposite edges simply supported. Appl. Math. Model. 36, 488–503. https://doi.org/10.1016/j.apm.2011.07.020.